A spectroscopic study of substituted anthranilic acids as sensitive environmental probes for detecting cancer cells

Culf, Adrian S.; Yin, Huimin; Monro, Susan; Ghosh, Anirban; Barnett, David A.; Ouellette, Rodney J.; Čuperlović-Culf, Miroslava; McFarland, Sherri A.

Publisher's version / Version de l'éditeur:
https://doi.org/10.1016/j.bmc.2015.12.044
Bioorganic and Medicinal Chemistry, 2015-12-29

Accepted Manuscript

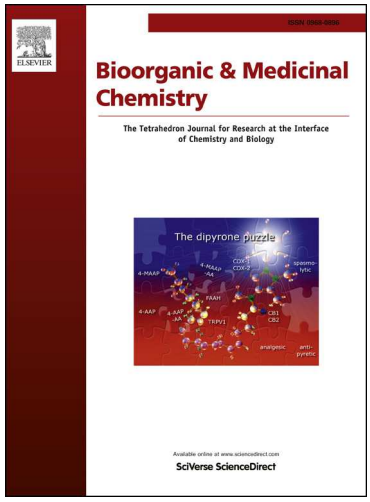

A Spectroscopic Study of Substituted Anthranilic Acids as Sensitive Environmental Probes for Detecting Cancer Cells

Adrian S. Culf, Huimin Yin, Susan Monro, Anirban Ghosh, David A. Barnett, Rodney J. Ouellette, Miroslava Čuperlović-Culf, Sherri A. McFarland

PII: S0968-0896(15)30210-8
DOI: http://dx.doi.org/10.1016/j.bmc.2015.12.044
Reference: BMC 12737

To appear in: *Bioorganic & Medicinal Chemistry*

Received Date: 5 November 2015
Revised Date: 18 December 2015
Accepted Date: 27 December 2015

Please cite this article as: Culf, A.S., Yin, H., Monro, S., Ghosh, A., Barnett, D.A., Ouellette, R.J., Čuperlović-Culf, M., McFarland, S.A., A Spectroscopic Study of Substituted Anthranilic Acids as Sensitive Environmental Probes for Detecting Cancer Cells, *Bioorganic & Medicinal Chemistry* (2015), doi: http://dx.doi.org/10.1016/j.bmc.2015.12.044

A Spectroscopic Study of Substituted Anthranilic Acids as Sensitive Environmental Probes for Detecting Cancer Cells

Adrian S. Culf,[†] Huimin Yin,[‡] Susan Monro,[‡] Anirban Ghosh,[†] David A. Barnett,[†] Rodney J. Ouellette,[†] Miroslava Čuperlović-Culf,[§] and Sherri A. McFarland[*‡]

[†]Atlantic Cancer Research Institute, Moncton, New Brunswick E1C 8X3, Canada; [‡]Department of Chemistry, Acadia University, Wolfville, Nova Scotia B4P 2R6, Canada; [§]National Research Council of Canada, Moncton, New Brunswick E1A 7R1, Canada

Small-molecule fluorescent reporters of disease states are highly sought after, yet they remain elusive. Anthranilic acids are extremely sensitive environmental probes, and hold promise as general but selective agents for cancer-cell detection if they can be equipped with the appropriate targeting groups. The optical properties of a small library of *N*-isopropyl invariant anthranilic acids were investigated in methanol and chloroform. Points of variation included: fluoro, trifluoromethyl, or cyano substitution on the aromatic ring, and derivitization of the parent carboxylic acid as esters or secondary carboxamides. Phenylboronic acid conjugation at the carboxylic acid alongside un-, mono-, and dimethylated 2-amino groups was also explored. The boron-containing anthranilic acids were also evaluated as sensitive fluorescent probes for cancer cells using laser scanning confocal microscopy. In general, the compounds produced blue fluorescence that was strongly influenced by substitution and environment. 4-Trifluoromethyl and 4-cyano esters proved to be the most sensitive environmental probes with quantum yields as large as 100% in chloroform, and enhancements of up to 30-fold on going from methanol to chloroform. Stokes shifts ranged from 63 to 120 nm, generally increasing with *ortho*-substitution and environmental polarity. It was demonstrated that phenylboronic acid conjugation was an attractive method for cancer cell detection via boronate ester formation with overexpressed glycoproteins (with no interference from normal, healthy cells), presumably due to favorable boron-sialic acid interactions.

INTRODUCTION

Ortho-aminobenzoic acid (compound **1**, Chart 1), also known as anthranilic acid, is a biosynthetic precursor to tryptophan that is also a valued chemical in a broad swathe of applications.[1] Anthranilic acid and its derivatives have been used as fragrances and dyes (*e.g.* indigo),[2] drug molecules,[3] fluorescent tags for oligosaccharides,[4] and fluorescent probes for peptides.[5,6] Its high quantum yield, small size, structural similarity to natural amino acids, and its ability to maintain favorable spectroscopic properties upon functionalization make anthranilic acid an excellent extrinsic fluorescent probe.[7] We have shown previously that this scaffold can be synthetically modified to include both electron-donating and electron-withdrawing groups on the core ring and derivatized at the carboxylic acid and amino functionalities.[8] Such changes are anticipated to improve the spectroscopic properties further and afford the opportunity to equip this reporter with targeting capacity for selective biological signaling. Herein we explore the optical properties of a variety of anthranilic acid derivatives and demonstrate that certain library members show promise as selective fluorescent probes for cancer cells.

Tumor-selective diagnostic agents rely on physiological differences between tumor cells and normal, healthy cells. The overexpression of certain cell-surface receptors and other biomarkers by tumor cells provides a convenient means for selective imaging of malignancies with fluorescent probes. Boron-based probes in particular have been of interest as early diagnostics for disease epitopes[9] due to their selective carbohydrate recognition via rapid and reversible interactions. Under biologically relevant conditions, boronic acids effectively bind 1,2- or 1,3-diols in monosaccharides, polysaccharides, and complex glycoproteins. Conjugation of boronic acids to fluorescent reporters has yielded robust sensors for cancer cell imaging. Salient examples include bisboronic acids tethered to π-stackable units separated by a linker.[10] Carbohydrate recognition by the boronic acid groups promotes π-stacking interactions that in turn lead to aggregation-induced emission (AIE). This rather complex probe design avoids the quenching effects that compromise fluorescent sensors. The use of anthranilic acids as reporters represents yet another motif for positive fluorescent signaling, and has the key advantage of being very simple in design and easily modified synthetically.

The reaction between boronic acid derivatives of certain anthranilic acid reporters and vicinal diols that present in sialic acids is expected to form cyclic boronate esters that are stable at physiological pH (Scheme 1). It has long been known that upregulation of sialyltransferase expression leads to aberrantly high levels of surface sialoglycans, which not only favor but possibly drive cancer metastasis.[11] Therefore, sialic acid-containing glycosphingolipids have attracted interest for almost 30 years in the search for drugs that can halt tumor growth and prevent metastasis.[12] We propose that terminal sialic acid residues, which are *N*- or O-

substituted derivatives of neuraminic acid, may also be viable targets for fluorescent reporting. Herein we investigate the fluorescence properties of a small library of anthranilic acids as well as the boronic acid conjugates of a few select members. We also highlight the utility of one of these conjugate reporters for selective cancer cell detection.

Scheme 1. Detection of Sialic Acid Residues via Boron-diol Exchange to Form Boronate Esters.

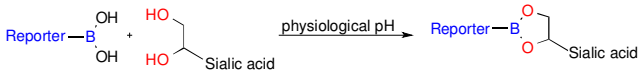

Anthranilic acids display a broad emission band centered near 380-420 nm. Having a large degree of charge-transfer (CT) character driven by the *ortho* amino and carboxylic acid groups,[13] this blue emission is extremely sensitive to changes in the molecular structure of the fluorophore and to its environment. Generally, such sensitivity is related to the degree of π delocalization giving rise to CT, and the magnitude of intramolecular charge transfer (ICT) between the ground and first singlet excited states. Both the identity of substituents and solvent effects influence ground- and excited-state geometries that either enhance or attenuate interactions such as intramolecular hydrogen bonding, which in turn affect π delocalization. Consequently, with judicious choice of substituents and targeting groups, it is possible to produce small-molecule fluorophores that undergo extraordinarily large changes in quantum yield and emission wavelength upon analyte binding. The purpose of the present study was to explore these factors, and to demonstrate that this class of fluorophores has utility in the search for selective probes for cancer-cell detection.

Chart 1. Anthranilic Acid Reporter Library.

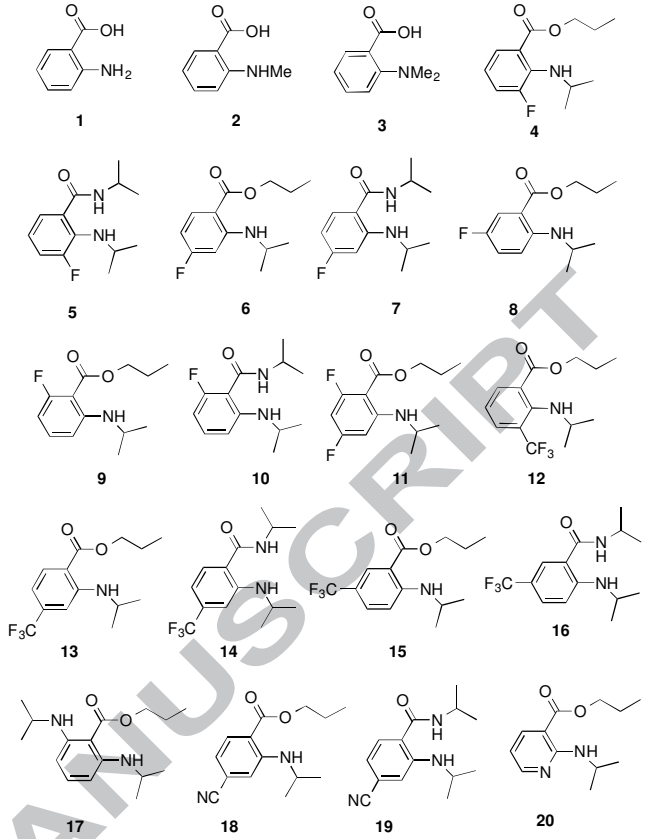

EXPERIMENTAL METHODS

Synthesis

Compounds 1-3 of this study were purchased from Alfa Aesar. The synthesis of 4-20 was reported recently by our group.[8] Nuclear magnetic resonance spectra were recorded on a Bruker Avance III 400 MHz spectrometer and referenced to the residual solvent peak for MeOH-d_4. High-resolution mass spectra (HRMS) were obtained using a Q-Exactive Quadrupole Orbitrap Mass Spectrometer.

(3-(2-Aminobenzamido)phenyl)boronic acid (***21***). To a solution of anthranilic acid (**1**) (137.1 mg, 1.0 mmol) and *N*,*N*-dimethylaminopyridine (61.1 mg, 0.5 mmol) in anhydrous CH_2Cl_2 (5 mL) was added *N*,*N*-dicyclohexylcarbodiimide (247.6 mg, 1.2 mmol), and the mixture was stirred for 30 min. 3-Aminobenzeneboronic acid (164.3 mg, 1.2 mmol) was then added in one portion, and the solution was stirred at room temperature for 18 hours. Following evaporation of the solvent, the solid was subjected to flash chromatography on silica with a linear 0-30% MeOH-CH_2Cl_2 gradient over 10 min, (typical elution 16% MeOH) to afford a light yellow gum (220 mg, 86%): ^{1}H NMR (MeOH-d_4, 400 MHz) δ 7.85 (m, 1H), 7.68 (m, 1H), 7.60 (m, 1H), 7.34 (m, 2H), 7.22 (m, 1H), 6.79 m, 1H), 6.68 (m, 1H), NH and OH signals exchanged with solvent; ^{13}C NMR (MeOH-d_4, 101 MHz) δ 170.5, 150.6, 139.3, 133.4, 130.4, 129.7, 129.4, 129.1, 123.9, 122.5, 118.2, 118.0, 117.4. HRMS (ESI+) *m/z* for $C_{13}H_{13}N_2O_3B$: calcd 257.1092, found 257.1083. λ_{abs} 255, 335 nm.

(3-(2-(Methylamino)benzamido)phenyl)boronic acid (***22***). To a solution of *N*-methylanthranilic acid (**2**) (151.1

mg, 1.0 mmol) and *N,N*-dimethylaminopyridine (61.1 mg , 0.5 mmol) in anhydrous CH_2Cl_2 (5 mL) was added *N,N*-dicyclohexylcarbodiimide (247.6 mg, 1.2 mmol) and stirred for 30 minutes. 3-Aminobenzeneboronic acid (164.3 mg, 1.2 mmol) was then added in one portion and the solution was stirred at room temperature for 18 hours. Following evaporation of the solvent, the solid was subjected to flash chromatography [silica, CH_2Cl_2/ MeOH 0-30% MeOH as a linear gradient over 10 minutes, typical elution 14% MeOH] to afford a light yellow gum (221 mg, 82%): ^{1}H NMR (MeOH-d_4, 400 MHz) δ 7.85 (m, 1H), 7.67 (m, 1H), 7.63 (m, 1H), 7.34 (m, 3H), 6.73 (m, 1H), 6.65 (m, 1H), 2.84 (s, 3H), NH and OH signals exchanged with solvent; ^{13}C NMR (MeOH-d_4, 101 MHz) δ 170.8, 151.8, 139.3, 134.0, 132.2, 130.4, 129.6, 129.1, 127.4, 123.9, 117.4, 115.9, 112.0, 29.9; HRMS (ESI+) *m/z* for $C_{14}H_{15}N_2O_3B$: calcd 271.1248, found 271.1239. λ_{abs} 260, 350 nm.

*(3-(2-(Dimethylamino)benzamido)phenyl)boronic acid (**23**).* To a solution of *N,N*-dimethylanthranilic acid (**3**) (165.2 mg, 1.0 mmol) and *N,N*-dimethylaminopyridine (61.1 mg , 0.5 mmol) in anhydrous CH_2Cl_2 (5 mL) was added *N,N*-dicyclohexylcarbodiimide (247.6 mg, 1.2 mmol) and stirred for 30 minutes. 3-Aminobenzeneboronic acid (164.3 mg, 1.2 mmol) was then added in one portion and the solution was stirred at room temperature for 18 hours. Following evaporation of the solvent, the solid was subjected to flash chromatography [silica, CH_2Cl_2/ MeOH 0-30% MeOH as a linear gradient over 10 minutes, typical elution 13% MeOH] to afford a light yellow gum (270 mg, 95%): ^{1}H NMR (MeOH-d_4, 400 MHz) δ 8.00 (m, 1H), 7.90 (m, 1H), 7.70 (m, 2H), 7.48 (m, 1H), 7.36 (m, 2H), 7.19 (m, 1H), 2.81 (s, 6H), NH and OH signals exchanged with solvent; ^{13}C NMR (MeOH-d_4) 101 MHz δ 167.3, 153.6, 139.2, 133.6, 131.7, 129.3, 129.2, 128.5, 126.3, 124.8, 123.5, 122.7, 121.1, 45.2. HRMS (ESI+) for $C_{15}H_{17}N_2O_3B$: calcd 285.1405, found 285.1395. λ_{abs} 285 nm.

Spectroscopy

Spectroscopic-grade methanol and chloroform were purchased from Caledon Laboratory Chemicals (Georgetown, Canada) and ACP Chemicals (Montreal, Canada), respectively. Compounds were prepared as 2 mM stock solutions in either methanol or chloroform and diluted accordingly for all spectroscopic measurements. Electronic absorption spectra were recorded using a JASCO V-530 spectrophotometer, and excitation/emission profiles were collected on a Photon Technology International (PTI) Quantamaster with real-time instrument response corrections applied within Felix32 software.

Molar extinction coefficients at wavelength maxima were determined as the slopes ε of linear fits of absorption versus concentration plots ($A=\varepsilon bc$) in the range of 100 μM down to 0.05 OD. At least five concentrations were used, with points measured in duplicate. Quantum yields for fluorescence emission (Φ_{em}) were measured relative to anthranilic acid (**1**) as the standard (s) at room temperature in aerated ethanol (Φ_f = 0.59)[13] according to Eq 1, where I, A, and η are integrated emission intensity, absorbance at the excitation wavelength, and refractive index of the solvent, respectively. Emission spectra were measured in triplicate using OD 0.05 at λ_{ex} (max) between 300–400 nm for each sample.

$$\Phi_{em} = \Phi_s \left(\frac{I}{A}\right)\left(\frac{A_s}{I_s}\right)\left(\frac{\eta^2}{\eta_s^2}\right) \quad (1)$$

Confocal microscopy

Cells were seeded on 8-well glass bottom chamber slides at a density of 2x10^4 cells mL^{-1} in 300 μL cell suspension per chamber, and allowed to grow overnight. After 12 h, the cell media was removed, and the cells were washed twice with cold media (without FBS) and twice with cold PBS. Compounds **21-23** (in DMSO stock solutions) were diluted to 10 μg mL^{-1} in PBS (<0.1% DMSO vehicle in working solution) and incubated with cells for 2 h at 4 °C. Controls were prepared in PBS with vehicle at the same percentage as in the samples and also incubated with cells under similar conditions. Following incubation with either compound or vehicle, the cells were washed twice with cold PBS, fixed with 70% EtOH (pre-cooled at -20 °C) for 5 min, and re-hydrated with two washes of PBS for 5-10 min each. The cells were then blocked for 30 min using 2-μm filtered 2% BSA in PBS, and counterstained for F-actin with Alexa Fluor® 594 Phalloidin (1:1000) in blocking buffer for 30 min at room temperature. Counter-stained cells were washed three times (10 min each) with PBS, mounted with PermaFluor Mountant Media (Shandon Immunon), and left in the dark overnight at room temperature. The cells were viewed with an Olympus FluoView™ FV1000 confocal microscope using FV10-ASW2.1 viewer software. Fluorescence emission was collected with $\lambda_{ex}/\lambda_{em}$ = 405/422 and 543/618 for **22** and Alexa Fluor® 594 Phalloidin, respectively.

RESULTS AND DISCUSSION

The anthranilic acids examined herein are shown in Chart 1. Compounds **4-20** were previously synthesized by us, and are substituted derivatives of commercially available **1-3**. Anthranilic acid-phenylboronic acids **21-23**, prepared in high yield (82 – 95%), were used to demonstrate the applicability of anthranilic acid fluorescence to bio-medical imaging of human cancer cells by confocal microscopy. The ring position of the *meta*-amine on the phenylboronic acid conjugator ensured maximum arylamine nucleophilicity whilst precluding steric interferences for secondary amide coupling. Also, the anthranilic acids were similarly unprotected, making use of the sterically challenging *ortho*-disubstitution to obviate complicating cross condensation reactions, which would lead to purification challenges. By exploiting such chemical features in DMAP-catalyzed DCC amide coupling conditions, we were able to prepare novel fluorescent boronic acid conjugates **21-23** (Scheme 2) without the need for additional protection-deprotection steps and in high yields (82-95% following flash chromatographic purification). Each new molecule was characterized by absorption spectroscopy, ^{1}H and ^{13}C NMR spectroscopy, and high-resolution mass spectrometry.

Scheme 2. Phenylboronic Acid Conjugates of Anthranilic Acid.

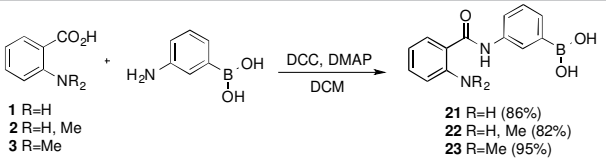

1 R=H
2 R=H, Me
3 R=Me

21 R=H (86%)
22 R=H, Me (82%)
23 R=Me (95%)

General Spectroscopic Trends. The steady-state absorption and fluorescence properties of compounds **1**-**20** (**21**-**23** discussed separately) were investigated in MeOH and $CHCl_3$ (Table 1) to identify promising candidates as reporters for sialic acid overexpression on cancer cells. These solvents were chosen to provide two distinct environments that would influence intramolecular hydrogen bonding (IHB) differently. It was anticipated that the polar protic MeOH would disrupt IHB networks more effectively than the less-polar aprotic $CHCl_3$. Others have studied and reported the general and specific solvent effects on the optical spectra of parent compound **1**.[7] In all solvents, its absorption profile is characterized by two dominant bands in the UV region: a shorter-wavelength benzenoid ππ* transition centered near 247 nm, and a longer-wavelength band near 336 nm that has been ascribed to a heterocyclic ππ* transition arising from an IHB framework.[13] In solvents that remain optically transparent down to 200 nm, an additional ππ* transition near 210 nm can also be discerned. In the present study, these peak maxima occurred at 210, 244, and 328 nm in MeOH and 240 and 336 nm in $CHCl_3$. Excitation throughout the UV gave rise to a broad, structureless ICT emission centered near 400 nm in MeOH and 407 nm in $CHCl_3$, consistent with previous reports and assigned to charge redistribution from the amino group to the electron-accepting carbonyl group.[13] Stokes shifts (Δλ) in these solvents were 71-72 nm, also supporting ICT accompanied by excited state conformational changes. The fluorescence quantum yields (Φ_{em}) for **1** in MeOH and $CHCl_3$ were 0.43 and 0.26, respectively. It has been hypothesized that the formation of the IHB in non-polar environments promotes non-radiative decay, thereby reducing emission quantum yields and lifetimes.[7] Presumably, the larger quantum yield measured for **1** in MeOH reflects a stronger fluorophore-solvent interaction with MeOH, and thus a weaker IHB.

A simple comparison of compounds **2** and **3** with **1** illustrates the dramatic effects that substitution can have on the solvatochromic properties of the anthranilic acid structure (Figure 1, Figure 2). For example, replacement of one hydrogen with a methyl group to form *N*-methylanthranilic acid **2** resulted in bathochromic (12 nm) and bathofluoric shifts (21 nm) in MeOH, but hypsochromic (20 nm) and hypsofluoric (39 nm) shifts in $CHCl_3$. These solvent-dependent differential trends gave rise to larger Stokes shifts in MeOH (Δλ=81 nm), and smaller Stokes shifts in $CHCl_3$ (Δλ=52 nm) relative to the parent compound. Methyl substitution reduced the quantum yields in both solvents by approximately 40%. With *N*,*N*-dimethyl substitution (**3**), the effects were even more profound. The longer-wavelength ππ* IHB absorption transition was completely abrogated, with a new peak discernible at 264 nm in MeOH and 274 nm in $CHCl_3$. ICT emission for **3** was diminished relative to **1** and **2** in $CHCl_3$ (Φ_{em}=0.05), and was not observed in MeOH. While a structured short-wavelength emission band centered at 298 nm could be discerned in MeOH, its intensity was too weak to determine a quantum yield. Consequently, *N*,*N*-dialkylation was not explored in the reporter library.

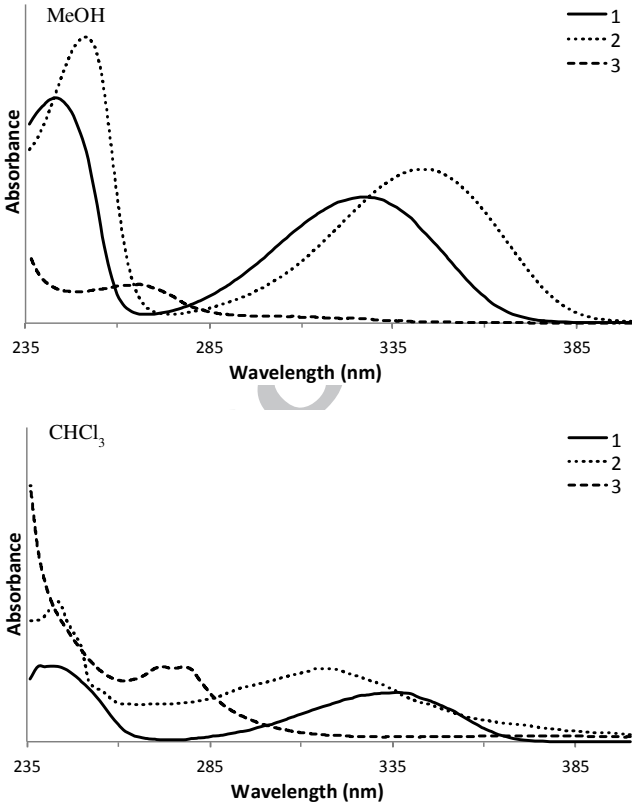

Figure 1. Absorbance spectra of commercially available anthranilic acids in two different solvents.

The library of reporters (**4**-**20**) prepared as part of this study yielded longest wavelength absorption maxima in the ranges of 310-382 nm in MeOH, and 338-384 nm in $CHCl_3$. Fluorescence emission maxima ranged from 407-480 in MeOH, and 400-453 nm in $CHCl_3$. It is interesting to note that while the absorption ranges generally red-shifted on going from MeOH to $CHCl_3$, the fluorescence emission ranges blue-shifted on going from MeOH to $CHCl_3$. In other words, $CHCl_3$ tended to red-shift the absorption spectra of the library members relative to MeOH, but blue-shift the emission spectra. There were several exceptions. Absorption spectra were completely solvent-independent for compounds **6**, **8**, and **11**, and mostly unchanged (±2 nm) for **12**, **13**, **15**, **17**, and **18**. Emission spectra were completely solvent-independent for **5**, **16**, and **19**, and mostly unchanged (±2 nm) for **4** and **20**. Also, the absorbance spectra of compounds **13**, **15**, and **17** were blue-shifted on going from MeOH to $CHCl_3$, but adhered to the more general trend observed for emission. Despite these exceptions, it is clear that the excited states populated upon photon absorption differ substantially from those that emit. This assertion is supported by the large Stokes shifts measured for the compounds: 63-120 nm in MeOH, and 57-92 nm in $CHCl_3$. Dissipation of energies up to 9000 cm^{-1} (typically between 0.5-1.2 eV) suggest that ICT state formation is facilitated by rather large conformational changes in rel-

atively small molecules, which is highly desirable for effective environmental sampling in biological applications. Such extreme sensitivity is unusual for small organic molecules, especially those with molecular weights below 250 (as indicated by a recent survey of small-molecule fluorescent probes).[14]

Quantum yields ranged from as low as 0.02 to 0.59 in MeOH, and 0.04 up to 1.0 in $CHCl_3$. For all library members, fluorescence quantum yields in $CHCl_3$ were larger than in MeOH. This difference was most pronounced for **13**, with Φ_{em}=0.03 in MeOH and unity in $CHCl_3$, corresponding to an increase of over 30-fold (Figure 3b). Together, the acute solvent-dependence of $\Delta\lambda$ and Φ_{em} for most of the reporters, their generally large Stokes shifts, and their small sizes make these compounds attractive fluorescent environmental probes, specifically for cancer cell detection.

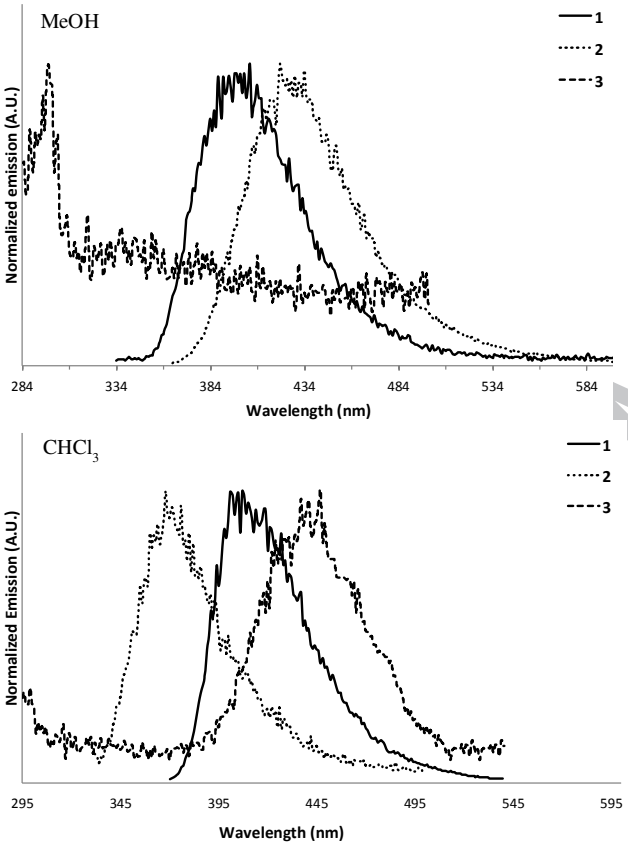

Figure 2. Normalized fluorescence emission of commercially available anthranilic acids in two different solvents.

Structure-Activity Spectroscopic Trends for Compounds 4-20). Compounds **4-19** display an invariant *N*-isopropyl group, with either *O*-propyl ester or *N*-isopropyl amide derivatization of the carboxylic acid of **1**. Fluorine, trifluoromethyl, and cyano groups were explored as electron withdrawing substituents at positions 3, 4, or 5 on the benzene skeleton. Other derivatives included 2,6-substitution with *N*-isopropylamine (**17**) and the use of a pyridine ring instead of benzene (**20**). From this relatively small library, some structure-activity trends emerged. It should be noted that all trifluoromethyl and cyano analogs of the fluoroaromatics were prepared, but only those with purity >99.9% were compared spectroscopically as part of this study.

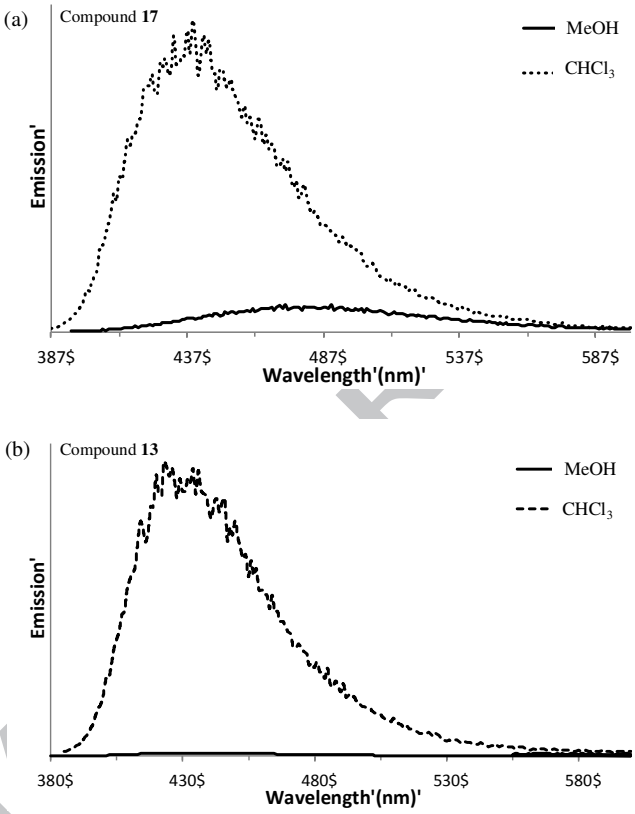

Figure 3. Fluorescence emission of compounds **17** (a) and **13** (b) in MeOH and in $CHCl_3$ excited at their excitation maxima with OD=0.05.

Stokes shifts were most pronounced in MeOH and are the basis for the present discussion, but the relative structure-activity trends were similar in $CHCl_3$. When a non-hydrogen substituent was present *ortho* to either the acid or amine functionality of the parent anthranilic acid, a marked increase in Stokes shift was observed. The largest shift ($\Delta\lambda$=120 nm) occurred for compound **5** in MeOH, which was fluoro-substituted *ortho* to the *N*-isopropylamine with *N*-isopropyl amide conjugation at C1. Within the fluorinated anthranilic acids, isopropyl amides at C1 gave larger Stokes shifts than the corresponding *O*-propyl esters: **5**>**4**, **10**>**9**, and **7**>**6**. Positioning of the fluorine at C4, *meta* to the *N*-isopropylamine reduced $\Delta\lambda$ to 69 nm, which was the smallest Stokes shift in the fluorinated series. With trifluoromethyl substitution, Stokes shifts as large as 96 nm were observed. As for the fluorinated series, isopropyl amides at C1 gave larger Stokes shifts than the corresponding *O*-propyl esters, **14**>**13** and **16**>**15**, and the smallest $\Delta\lambda$ was 69 nm for **13** and **15**. C4-Cyano substitution of both the *N*-isopropyl amide and the *O*-propyl ester anthranilic acids gave intermediate Stokes shifts (71-84 nm), while C6-*N*-isopropyl substitution of the *N*-isopropyl amide (**17**) produced the second largest Stokes shift of 106 nm. Replacement of the benzene ring with pyridine diminished $\Delta\lambda$ to 63 nm.

While compounds **4-20** all produce emission in the blue region of the electromagnetic spectrum, noticeably

longer wavelength fluorescence emission (>440 nm) was observed for the following compounds in MeOH: **8** (445 nm), **11** (445 nm), **17** (480 nm), **18** (453 nm), and **19** (452 nm). Qualitatively, it appeared that emission wavelength was red-shifted in the order: *N*-isopropyl > cyano > fluoro > trifluoromethyl. Within the fluorinated series, *O*-propyl esters produced the longest-wavelength emission, which was near 445 nm in MeOH. The cyano-substituted series produced emission as long as 453 nm, which was independent of the carboxylic acid functionalization, and anthranilic acid derivative **17** with the *O*-propyl ester flanked by two *N*-isopropyl groups produced the longest-wavelength emission of all compounds investigated (480 nm in MeOH, Figure 3a). Emission by compound **17** was also the most sensitive to environment ($\Delta\lambda[CHCl_3\text{-MeOH}]$ = 41 nm). Trifluoromethyl substitution resulted in the shortest-wavelength emission regardless of the carboxylic acid functionalization. Nevertheless, substitution at any position with any of these groups shifted the emission bathochromically relative to the parent anthranilic acid **1**. While it is difficult to predict the most favorable transition dipoles for the various substitution patterns without knowledge of their ground-state geometries, bathochromic shifts determined from empirical measurements shed light on those structures that promote excited-state ICT. In the case of compound **17**, the 480-nm emission in MeOH shifted to 439 nm in $CHCl_3$ (Figure 3a), suggesting that environment plays a crucial role in the degree of ICT with some substitution patterns. A shift in emission of over 40 nm in response to a change in environment has potential utility for ratiometric imaging.

Six compounds produced quantum yields greater than the parent anthranilic acid in MeOH or $CHCl_3$: **4** (0.63), **8** (0.81), **13** (1.00), **15** (0.82), **18** (0.88), and **20** (0.76), all in $CHCl_3$. In general, *O*-propyl esters produced the larger quantum yields. Each substituent subset yielded at least one member with a quantum efficiency over 80%. Importantly, Φ_{em} proved to be extremely sensitive to solvent for a variety of the compounds investigated. Trifluoromethyl substitution gave the largest solvent-dependent Φ_{em}, with emission in $CHCl_3$ being over 30-fold stronger than in MeOH for compound **13** (Figure 3b). Cyano-substitution (compound **17**) at the same position followed with a $CHCl_3$/MeOH Φ_{em} ratio of approximately. *Para* substitution of the electron-withdrawing substituent relative to the *O*-propyl ester appeared to maximize this effect, except in the case of fluorine, which produced the smallest differences in Φ_{em} between MeOH and $CHCl_3$. The enhanced quantum yields observed in less polar environments is an attractive feature for biological signalling of hydrophobic receptor-ligand interactions, whereby a lack of fluorescence in polar protic environments is advantageous for minimizing background fluorescence.

Spectroscopic Properties of Phenylboronic Acid Conjugates of Anthranilic Acid. The reporter library indicated that conversion of the carboxylic acid of **1** to the corresponding *O*-propyl ester or *N*-isopropyl amide did not compromise the favourable fluorescence properties of many of the anthranilic acid derivatives. Therefore, an amide linkage was used to conjugate phenylboronic acids to the anthranilic acid reporter groups **1-3** in order to determine the feasibility of selective cancer cell detection with such simple architectures. Compounds **21-23** (Scheme 2) are phenylboronic acid analogs of **1-3**. As expected, substitution altered the absorption and emission profiles of the boronic acid conjugates relative to their parent structures (Table 1), and the effects depended on the neighboring amino group. The molar extinction coefficients taken at the longest wavelength absorption maxima were diminished for **21** relative to **1** in both MeOH and $CHCl_3$; attenuated for **22** relative to **2** in MeOH, but enhanced in $CHCl_3$; and significantly enhanced for **23** relative to **3** in both solvents (Supporting Information, Figures S1, S3, and S4). Clearly, mono- and dimethyl substitution of the *ortho*-amino group influence the optical properties of the conjugates. Relative to the parent anthranilic acid, the absorption spectrum of compound **20** was blue-shifted by 38 nm in $CHCl_3$ and remained relatively unchanged in MeOH. For **21** and **22**, the changes were slight in both solvents but bathochromic. For compounds **20** and **21**, the absorbance spectra were hypsochromically shifted by 32 and 26 nm, respectively, on going from MeOH to $CHCl_3$. By contrast the absorbance shift for **22** was bathochromic and marginal (6 nm).

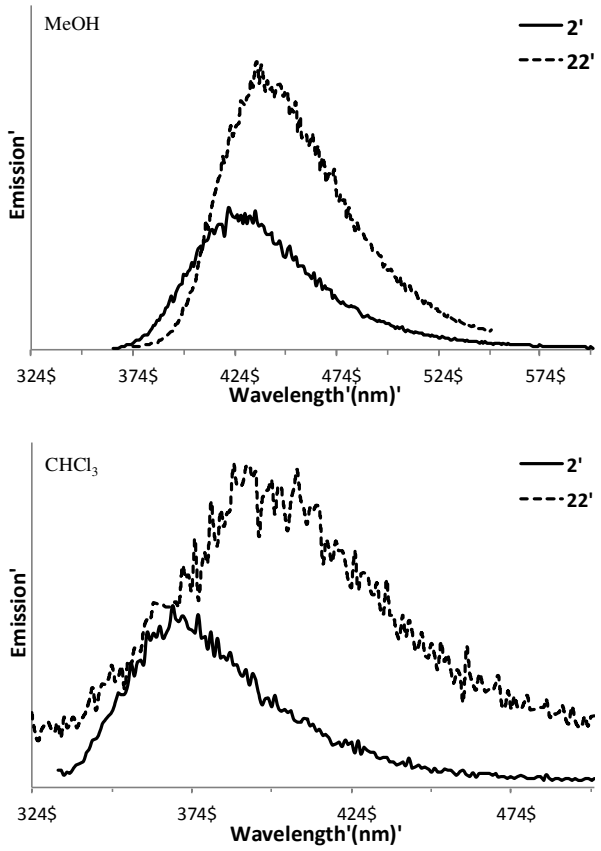

Figure 4. Fluorescence emission produced by phenylboronic acid conjugate **22** compared to the parent derivative **2** in MeOH and $CHCl_3$.

The fluorescence emission maxima for the conjugates were longest for compounds **21** and **22** in MeOH (435 nm), and shortest for **23** in MeOH (326 nm). Relative to the parent compounds, the emission maxima for the conjugates were red-shifted except for compound **23** in

$CHCl_3$ (Figure 4, and Supporting Information Figures S2 and S5). They were blue-shifted on going from MeOH to $CHCl_3$ except for compound **23**. It is clear that *N,N*-dimethyl substitution of the *ortho*-amino group results in excited state properties that are significantly different than the 1° and 2° amines, perhaps due to nonradiative photoinduced electron transfer pathways with increased electron-donating capacity. The quantum yields for emission also reflected these differences, with Φ_{em} only 3-4% for **23** in the two solvents, similar to what was observed for **3**. Quantum yields measured for **21** in both solvents were half of what they were for the parent complexes, but still 10-26%. Interestingly, Φ_{em} for conjugate **22** increased relative to **2** in both MeOH and $CHCl_3$, and was more than 60% in MeOH (Figure 4). The Stokes shifts for **22** were also larger relative to the parent, 89 nm in MeOH and 72 nm in $CHCl_3$. Unlike many of the reporter library members that emitted more strongly in $CHCl_3$ (Figure 3), the fluorescence quantum yield measured for **22** decreased, albeit only slightly, on going from MeOH to $CHCl_3$ (64% vs. 47%). Due to its bright fluorescence signal and relatively large Stokes shift, compound **22** was studied further as a fluorescent probe for cancer cells.

Cancer Cell Detection with a Phenylboronic Acid Conjugate. We hypothesized that phenylboronic acids conjugated to an appropriate fluorescent reporter would be capable of forming cyclic boronate esters with terminal sialic acid residues on cancer cells. Because these groups containing the requisite vicinal diol are preferentially expressed on cancer cell surfaces,[15] selective detection of cancer cells should be possible in the presence of normal, healthy cells. As proof of concept, metastatic SKBR3 breast cancer cells were exposed to phenylboronic acid **22** and counterstained with Alexa Fluor® 594 Phalloidin. The purpose of the counterstain was to make the cells visible under the fluorescence microscope under all conditions. When examined with 405-nm laser excitation using a confocal microscope, the cells emitted blue fluorescence while excitation at 543 nm produced red emission from the F-actin counterstain (Figure 5a-c). In order to ascertain whether **22** was selective for cancer cells, "healthy" cells were also exposed to the phenylboronic acid conjugate and counterstained in the same manner. The noncancerous MCF10A breast cell line showed no detectable blue fluorescence with 405-nm excitation (Figure 5b-f) while the counterstain produced the expected red emission with 543-nm excitation. Other cancer cell types were also investigated to confirm that the blue fluorescence observed for the highly metastatic SKBR3 cells was a general phenomenon that could be applied to a variety of malignant phenotypes (Figure 6). All cancer cells exposed to **22** produced blue emission (pseudocolored green in Figure 6, right panel), including other highly metastatic breast cancer cells (MDA-MB-231) as well as colon cancer cells (HCT116 colorectal carcinoma, DLD-1 Dukes' Type C colorectal adenocarcinoma). Even the less aggressive MCF7 breast cancer and HT1018 fibrosarcoma cell lines could be detected readily with compound **22**.

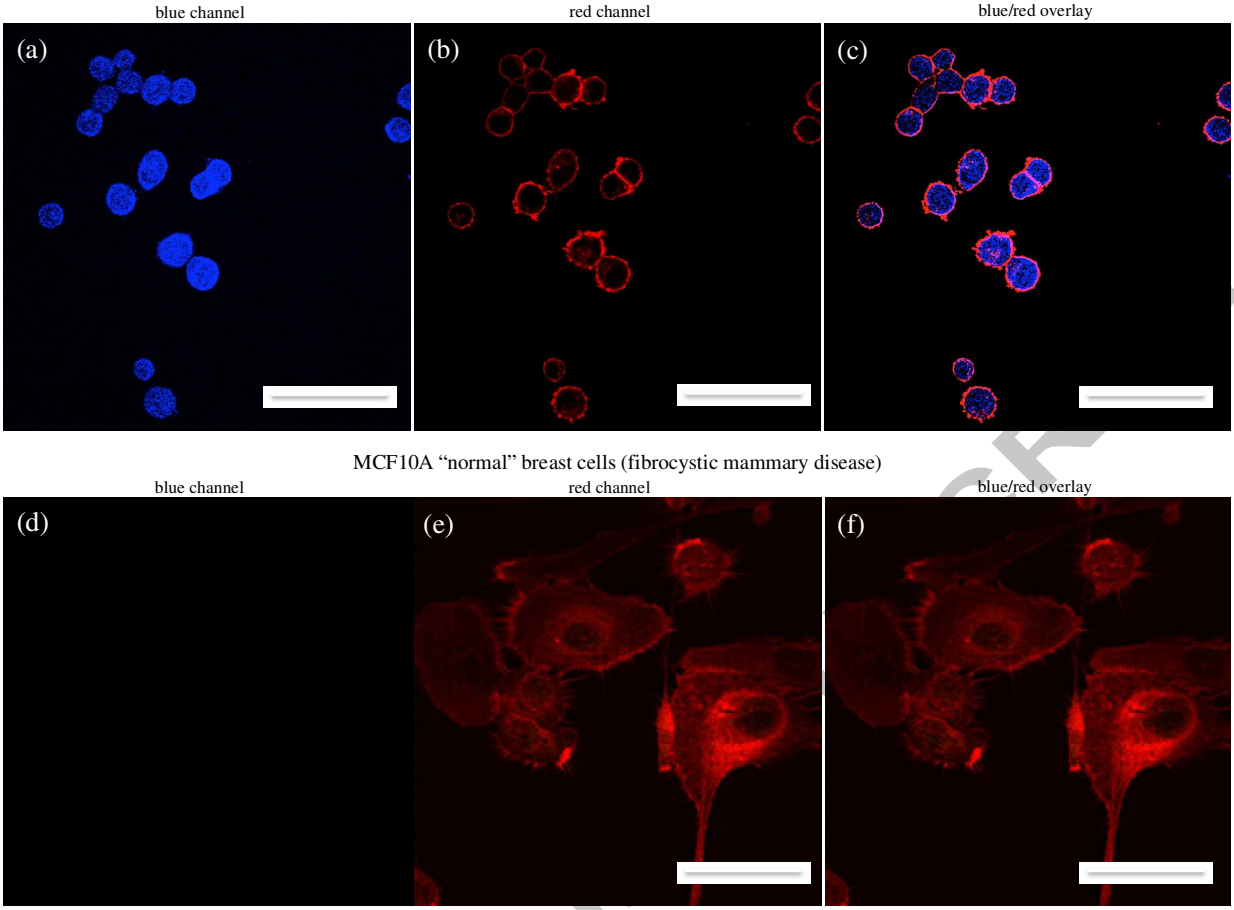

Figure 5. Laser scanning confocal microscopy images of SKBR3 breast cancer cells (top panel) and normal MCF10A breast cells stained with compound **22** (blue fluorescence) and counterstained for F-actin with Alexa Fluor® 594 Phalloidin (red fluorescence). Images (a) and (d) were collected with $\lambda_{ex}/\lambda_{em}$ = 405/422 nm, and images (b) and (e) were viewed with $\lambda_{ex}/\lambda_{em}$ = 543/618 nm. Images (c) and (f) are the corresponding blue/red overlays [(a)+(b) and (d)+(e), respectively]. The scale bar is 50 μm (MCF10A cells have a large size variation relative to SKBR3 cells).

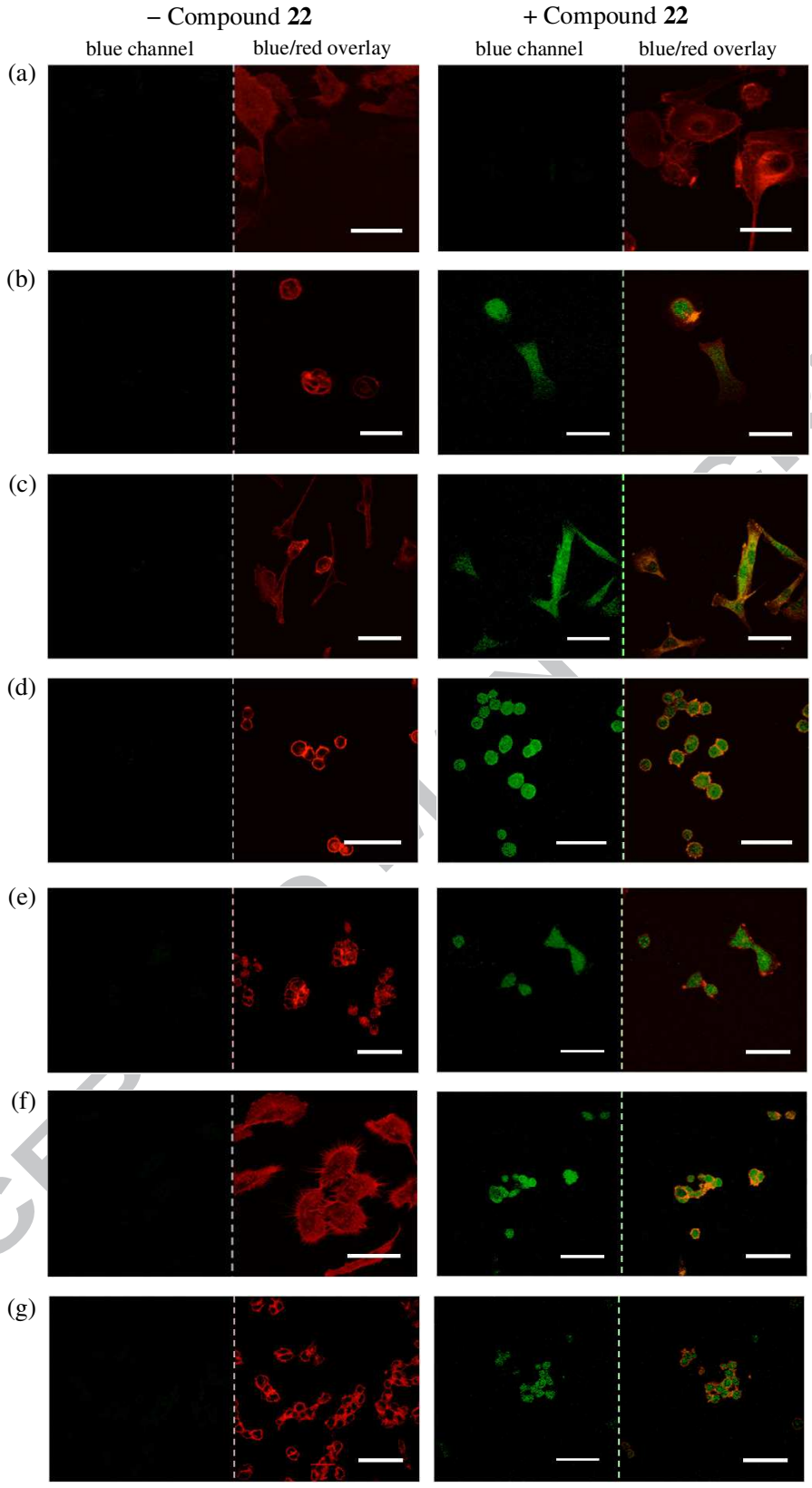

Figure 6. Laser scanning confocal microscopy images of cells counterstained with Alexa Fluor® 594 Phalloidin (red fluorescence) in the absence (left panel) or presence (right panel) of compound **22**: (a) MCF10A "normal" breast cells (fibrocystic mammary disease), (b) MCF7 nonaggressive but metastatic breast cancer cells (adenocarcinoma, pleural effusion), (c) MDA-MB-231 highly metastatic breast cancer cells (adenocarcinoma, pleural effusion), (d) SKBR3 highly metastatic breast cancer cells (adenocarcinoma, pleural effusion), (e) DLD-1 colorectal cancer cells (Duke's Type C, adenocarcinoma), (f) HCT116 colorectal cancer cells (carcinoma), and (g) HT1080 connective tissue cancer cells (fibrosarcoma). The blue fluorescence from

compound **22** is pseudocolored green; the scale bar is 50 μm (except for (f) left panel, where it is 15 μm). Selected regions are representative of entire samples.

Table 1. Optical Properties of Compounds 1-23. N.D. = Not Determined.

Compound	Solvent	λ_{abs} (log ε), nm	λ_{em} (nm)	Stokes shift Δλ (nm)	Quantum yield Φ_{em}
1	MeOH	210 (3.76), 244 (3.19), 328 (2.98)	400	72	0.43
	$CHCl_3$	240 (2.81), 336 (2.54)	407	71	0.26
2	MeOH	216 (3.80), 250 (3.29), 340 (3.04)	421	81	0.27
	$CHCl_3$	244 (3.11), 316 (2.85)	368	52	0.15
3	MeOH	218 (3.31), 264 (2.40)	298	34	N.D.
	$CHCl_3$	274 (2.85)	447	173	0.05
4	MeOH	218 (3.60), 250 (4.13), 346 (2.85)	436	90	0.44
	$CHCl_3$	252 (3.24), 350 (2.98)	426	76	0.63
5	MeOH	210 (3.85), 242 (3.45), 310 (2.93)	430	120	0.03
	CHCl3	250 (3.16), 302 (2.54), 338 (2.54)	430	92	0.11
6	MeOH	218 (3.64), 256 (3.28), 338 (3.00)	407	69	0.39
	$CHCl_3$	260 (3.19), 338 (2.93)	400	62	0.52
7	MeOH	208 (3.67), 256 (3.42), 326 (2.98)	409	83	0.10
	$CHCl_3$	264 (3.45), 338 (3.06)	404	66	0.15
8	MeOH	218 (3.48), 254 (3.10), 368 (2.98)	445	77	0.59
	$CHCl_3$	2.54 (2.60), 368 (2.54)	440	72	0.81
9	MeOH	224 (3.60), 250 (3.22), 346 (2.95)	434	88	0.35
	$CHCl_3$	254 (3.06), 350 (2.81)	423	73	0.53
10	MeOH	210 (3.46), 248 (3.23), 322 (2.70)	426	104	0.09
	$CHCl_3$	254 (3.31), 344 (2.95)	417	73	0.29
11	MeOH	206 (3.57), 2.94 (2.85), 350 (3.04)	445	95	0.15
	$CHCl_3$	296 (2.65), 350 (2.81)	420	70	0.26
12	MeOH	218 (3.48), 264 (3.10), 338 (2.70)	434	96	0.02
	$CHCl_3$	268 (3.13), 340 (2.70)	428	88	0.04
13	MeOH	222 (3.63), 256 (3.33), 366 (3.08)	435	69	0.03
	$CHCl_3$	260 (3.34), 364 (3.11)	429	65	1.00
14	MeOH	214 (3.53), 258 (3.33), 350 (2.90)	438	88	0.25

	$CHCl_3$	258 (3.33), 356 (2.93)	436	80	0.30
15	MeOH	218 (3.79), 262 (3.60), 350 (3.15)	419	69	0.58
	$CHCl_3$	264 (3.38), 348 (2.95)	414	66	0.82
16	MeOH	214 (3.81), 264 (3.69), 334 (3.11)	416	82	0.05
	$CHCl_3$	270 (3.54), 340 (3.00)	416	76	0.20
17	MeOH	210 (3.24), 298 (2.48), 374 (2.65)	480	106	0.13
	$CHCl_3$	252 (3.10), 372 (2.93)	439	67	0.50
18	MeOH	234 (3.87), 258 (3.36), 382 (3.06)	453	71	0.11
	$CHCl_3$	260 (3.48), 384 (3.20)	443	59	0.88
19	MeOH	228 (3.69), 260 (3.31), 368 (2.90)	452	84	0.16
	$CHCl_3$	264 (3.43), 376 (3.04)	453	77	0.43
20	MeOH	202 (3.50), 252 (2.90), 346 (3.02)	409	63	0.49
	$CHCl_3$	256 (3.31), 350 (3.02)	407	57	0.76
21	MeOH	212 (3.22), 250 (2.74), 330 (2.40)	435	105	0.26
	$CHCl_3$	240 (3.02), 298 (2.60)	418	120	0.10
22	MeOH	210 (3.34), 254 (3.00), 346 (2.54)	435	89	0.64
	$CHCl_3$	320 (3.10)	392	72	0.47
23	MeOH	218 (3.48), 250 (3.13), 272 (3.10)	326	54	0.04
	$CHCl_3$	254 (3.27), 278 (3.30)	378	100	0.03

CONCLUSION

The absorption and fluorescence properties of 17 previously synthesized anthranilic acid derivatives and 3 new phenylboronic acid conjugates were described and compared to the parent structures. It was found that solvatochromic effects were greatest for the *O*-propyl ester derivatives of anthranilic acid, and that ICT in the excited state was largest for compound **17**, characterized by di-substitution with *N*-isopropyl *ortho* to the ester. Differential quantum yields in $CHCl_3$ versus MeOH were more than 30-fold for **13**, and 8-fold for **18**, with *para*-substitution of a trifluoromethyl or cyano group relative to the ester. Such solvent-dependent optical properties open up the possibility of intensity-based and ratiometric reporting for this class of small-molecule organic fluorophores. We also demonstrated that it is possible to detect cancer cells based on fluorescence emission from a phenylboronic acid conjugate of an anthranilic acid derivative. The reporter was selective for cancer cells. While this investigation did not involve further mechanistic studies in cells, boronate ester formation between **22** and sialic acid residues on the cancer cells could be directly responsible for the fluorescence signal. This interaction may prove to be a general interaction for selective fluorescent reporting, and future boronic acid conjugates could be designed as theranostic agents.

ASSOCIATED CONTENT

Supporting Information. UV-Vis absorption and fluorescence emission spectra for selected anthranilic acid derivatives. This material is available free of charge via the Internet at http://pubs.acs.org.

AUTHOR INFORMATION

Corresponding Author

Email for S.A.M.: sherri.mcfarland@acadiau.ca; Email for A.C.: adrianc@canceratl.ca

ACKNOWLEDGMENT

A.C. thanks ACRI and NRC for financial support, and Prof. M. Touaibia for NMR access. S.A.M. thanks the Natural Sciences and Engineering Council of Canada, the Canadian

Foundation for Innovation, the Nova Scotia Research and Innovation Trust, and Acadia University for financial support.

REFERENCES

(1) Walsh, C. T.; Haynes, S. W.; Ames, B. D. *Nat. Prod. Rep.* **2012**, *29* (1), 37–59.
(2) Wiklund, P.; Bergman, J. *Curr. Org. Synth.* **2006**, *3* (3), 379–402.
(3) Horton, D. A.; Bourne, G. T.; Smythe, M. L. *Chem. Rev.* **2003**, *103* (3), 893–930.
(4) Saddic, G. N.; Dhume, S. T.; Anumula, K. R. *Methods Mol. Biol. Clifton NJ* **2008**, *446*, 215–229.
(5) Turchiello, R. F.; Lamy-Freund, M. T.; Hirata, I. Y.; Juliano, L.; Ito, A. S. *Biophys. Chem.* **1998**, *73* (3), 217–225.
(6) Ito, A. S.; Turchiello, R. D.; Hirata, I. Y.; Cezari, M. H.; Meldal, M.; Juliano, L. *Biospectroscopy* **1998**, *4* (6), 395–402.
(7) Takara, M.; Ito, A. S. *J. Fluoresc.* **2005**, *15* (2), 171–177.
(8) Culf, A. S.; Čuperlović-Culf, M.; Ouellette, R. J.; Decken, A. *Org. Lett.* **2015**.
(9) Pappin, B.; Kiefel, M. J.; Houston, T. A. *Boron-Carbohydrate Interactions*; InTech, 2012.
(10) Sun, X.; Fossey, J. S.; Zhai, W.; James, T. D. *Chem. Commun.* **2015**, DOI: 10.1039/C5CC08633G.
(11) Fredman, P.; Hedberg, K.; Brezicka, T. *BioDrugs Clin. Immunother. Biopharm. Gene Ther.* **2003**, *17* (3), 155–167.
(12) Jayant, S.; Khandare, J. J.; Wang, Y.; Singh, A. P.; Vorsa, N.; Minko, T. *Pharm. Res.* **2007**, *24* (11), 2120–2130.
(13) Stalin, T.; Rajendiran, N. *J. Photochem. Photobiol. Chem.* **2006**, *182* (2), 137–150.
(14) Terai, T.; Nagano, T. *Pflüg. Arch. Eur. J. Physiol.* **2013**, *465* (3), 347–359.
(15) Varki, N. M.; Varki, A. *Lab. Invest.* **2007**, *87* (9), 851–857.

Table of Contents artwork